Applied Surface Science 406 (2017) 178–185

Contents lists available at ScienceDirect

Applied Surface Science

journal homepage: www.elsevier.com/locate/apsusc

Micromechanism of oxygen transport during initial stage oxidation in Si(100) surface: A ReaxFF molecular dynamics simulation study

Yu Sun [a,b,*], Yilun Liu [c], Xuefeng Chen [a], Zhi Zhai [a], Fei Xu [b], Yijun Liu [b,d]

[a] State Key Laboratory for Manufacturing Systems Engineering, School of Mechanical Engineering, Xi'an Jiaotong University, Xi'an 710049, China
[b] Institute for Computational Mechanics and Its Applications, Northwestern Polytechnical University, Xi'an 710072, China
[c] State Key Laboratory for Strength and Vibration of Mechanical Structures, School of Aerospace Engineering, Xi'an Jiaotong University, Xi'an 710049, China
[d] Mechanical Engineering, University of Cincinnati, Cincinnati, OH 45221-0072, USA

ARTICLE INFO

Article history:
Received 25 September 2016
Received in revised form
20 December 2016
Accepted 30 January 2017
Available online 9 February 2017

Keywords:
ReaxFF MD
Oxygen transport
Oxidation
Thermal actuation

ABSTRACT

The early stage oxidation in Si(100) surface has been investigated in this work by a reactive force field molecular dynamics (ReaxFF MD) simulation, manifesting that the oxygen transport acted as a dominant issue for initial oxidation process. Due to the oxidation, a compressive stress was generated in the oxide layer which blocked the oxygen transport perpendicular to the Si(100) surface and further prevented oxidation in the deeper layer. In contrast, thermal actuation was beneficial to the oxygen transport into deeper layer as temperature increases. Therefore, a competition mechanism was found for the oxygen transport during early stage oxidation in Si(100) surface. At room temperature, the oxygen transport was governed by the blocking effect of compressive stress, so a better quality oxide film with more uniform interface and more stoichiometric oxide structure was obtained. Indeed, the mechanism presented in this work is also applicable for other self-limiting oxidation (e.g. metal oxidation) and is helpful for the design of high-performance electronic devices.

© 2017 Elsevier B.V. All rights reserved.

1. Introduction

The oxidation of Si(100) has drawn numbers of attentions because it is a fundamental factor of surface chemical reaction [1,2]. The Si/SiO_2 interface also shows significance to the fabrication and application of silicon-based devices such as metal-oxide-semiconductor field-effect transistors. During oxidation process, inserting of O atoms can cause surface layers to expand which is constrained by substrate, inducing tensile strain in Si and compressive one in SiO_2. Such residual compressive stress in oxide film causes the so-called "self-limiting oxidation" since the barrier led by compressive deformation is higher than the activation energy of oxygen diffusion and reaction [3,4]. Besides, stress distributions and the related interface states are even more important to the performance of the device as the film thickness decreases to nano-scale, which are closely linked to the initial oxidation process [5,6].

For the oxidation of Si, various experimental methods have been proposed [7–11]. Some experiments discussed the effects of external stress on Si oxidation and revealed that the oxidation was usually promoted by tensile stress [12–20]. On the other hand, the oxide growth and interface structure have been studied by first-principles calculations [21–24]. However, expensive computation cost kept the first-principles calculations far away from the large-scale dynamics. With the purpose of realizing large-scale simulation on thermal oxidation process of Si, classical MD with variable charge interatomic potential as well as charge-transfer interatomic potential based on Tersoff type have been developed and utilized [25,26]. To obtain in-depth understanding of the oxidation process and microstructure evolution, several studies have focused on the early stage oxidation by using a ReaxFF MD simulation via a sophisticated bond-order potential which was established by the group of Adri van Duin [5,6,27–33]. Among these studies, hyperthermal oxidation has been well investigated involving detailed reaction mechanism, temperature effect and interface structures [27,28,30–32]. For the conventional thermal oxidation, Mauludi et al. provided the viability of ReaxFF MD method for the atomic simulation of Si oxidation, and gave the related results on dry oxidation as well as wet oxidation of Si(100) surface [5,6]. Haining et al. in the same group focused on the effect of external strain [29]. In the pervious studies of the Si oxidation, including ReaxFF

* Corresponding author at: State Key Laboratory for Manufacturing Systems Engineering, School of Mechanical Engineering, Xi'an Jiaotong University, Xi'an 710049, China.
E-mail address: yu.sun@xjtu.edu.cn (Y. Sun).

http://dx.doi.org/10.1016/j.apsusc.2017.01.302
0169-4332/© 2017 Elsevier B.V. All rights reserved.

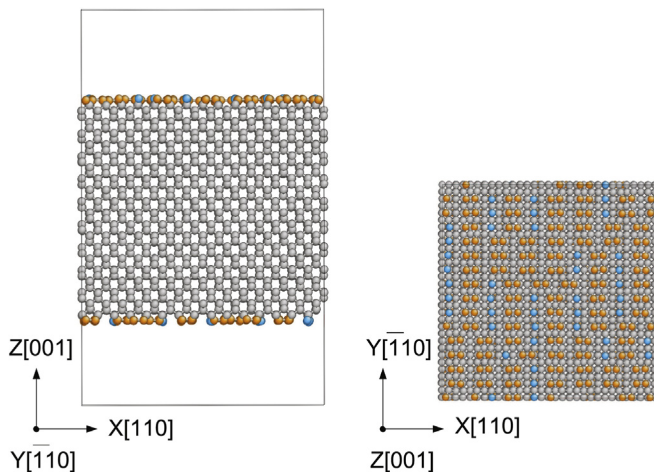

Fig. 1. Side view and top view of relaxed Si crystal. The dangling bonds of Si(100) surface formed dimers by structure relaxation, indicating by orange atoms with coordination number as 3. Light gray and light blue indicate coordination number of Si as 4 and 2, respectively. (For interpretation of the references to color in this figure legend, the reader is referred to the web version of this article.)

MD simulation, quantum MD simulation and earlier experimental results, the ballistic transport of O atoms was indicated to be the dominant factor for initial oxidation [34,35]. Despite several efforts on investigating the early stage of Si oxidation, mechanism on how thermal effect and intrinsic stress influence the transport of O atoms has not been clearly discussed.

To address such a crucial issue, we used the ReaxFF MD to examine the oxidation behavior of Si under different temperatures ranging from 300 K to 1200 K via atomic-scale perspective, concentrating on the micromechanism of early stage oxidation. We have found that the O transport was dominated by the competition between thermal actuation and compressive stress blocking. The quality of oxide film under different temperatures was also analyzed.

Table 1
Lattice constant, cohesive energy, elastic modulus and bulk modulus of crystalline Si calculated by ReaxFF MD, comparing with results from *ab initio* density functional calculation and experiment.

	ReaxFF MD	*Ab initio* [36]	Experiment [36]
Lattice constant (nm)	0.532	0.545	0.543
Cohesive energy (eV/atom)	4.57	4.84	4.63
	ReaxFF MD	Experiment [37]	
Elastic modulus (GPa)	113.3	130	
Bulk modulus (GPa)	111	97.8	

2. Computational details

All the simulations were conducted with the open-source LAMMPS code integrated with ReaxFF [38,39]. The force field parameters used in this work were developed by Buehler et al. which provided accurate description on the interaction between Si and oxygen gas [40]. Recently, these parameters have been utilized to simulate the thermal oxidation of Si, showing good agreement with experiment results [41].

With the purpose of performing model validation, crystalline properties including lattice constant and cohesive energy were calculated by statics relaxation and NPT (isothermal–isobaric) ensemble, summarizing in Table 1 reasonably agree with *ab initio* density functional calculation and experiment. By imposing a uniaxial tension on the simulation box after totally relaxed the stress of Si(100) bulk by NPT ensemble, the elastic modulus, i.e. the gradient of stress–strain curve, was calculated as 113.3 GPa. Additionally, the bulk modulus was calculated following its definition, obtained as 111 GPa. Both of the values are listed in Table 1, similar to the previous experimental results [37]. The discrepancy may come from much higher strain rate of the present MD simulation.

To perform the simulation, a bulk Si containing 9000 atoms sizing 56.4 Å × 56.4 Å × 51.9 Å was set up, with [110] and [$\bar{1}$10] as *x*-axis and *y*-axis, [001] as *z*-axis, respectively. The simulation box was set as 86.4 Å along *z* direction to obtain Si(100) free surface and give space for oxygen gas. Periodic boundary conditions were applied to all three directions.

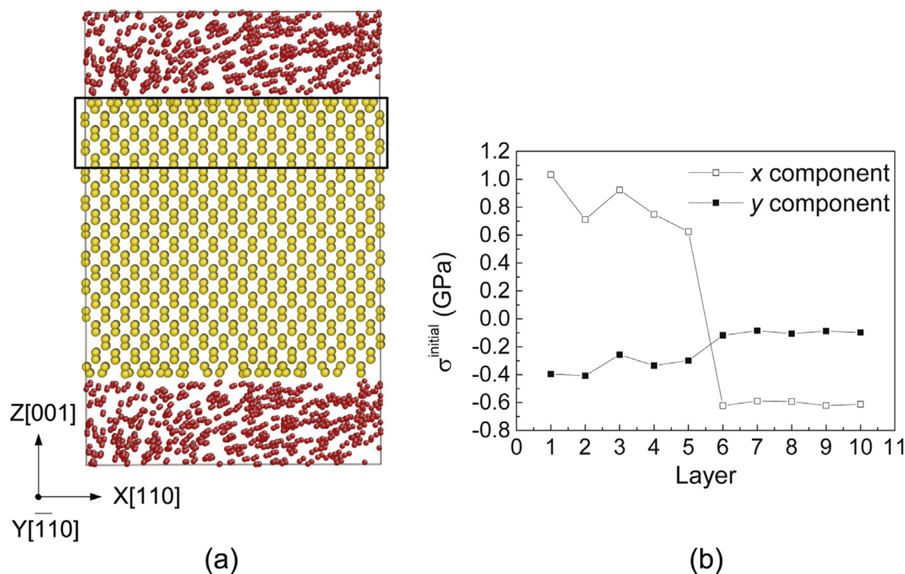

Fig. 2. (a) Initial model for Si(100) oxidation containing both O_2 molecules and Si crystal. Red and yellow atoms are O and Si, respectively. (b) The distribution of *x* and *y* component residual stress along *z* direction in the region marked by a box in (a), caused by the free surface of Si(100) and the interaction between Si and O. (For interpretation of the references to color in this figure legend, the reader is referred to the web version of this article.)

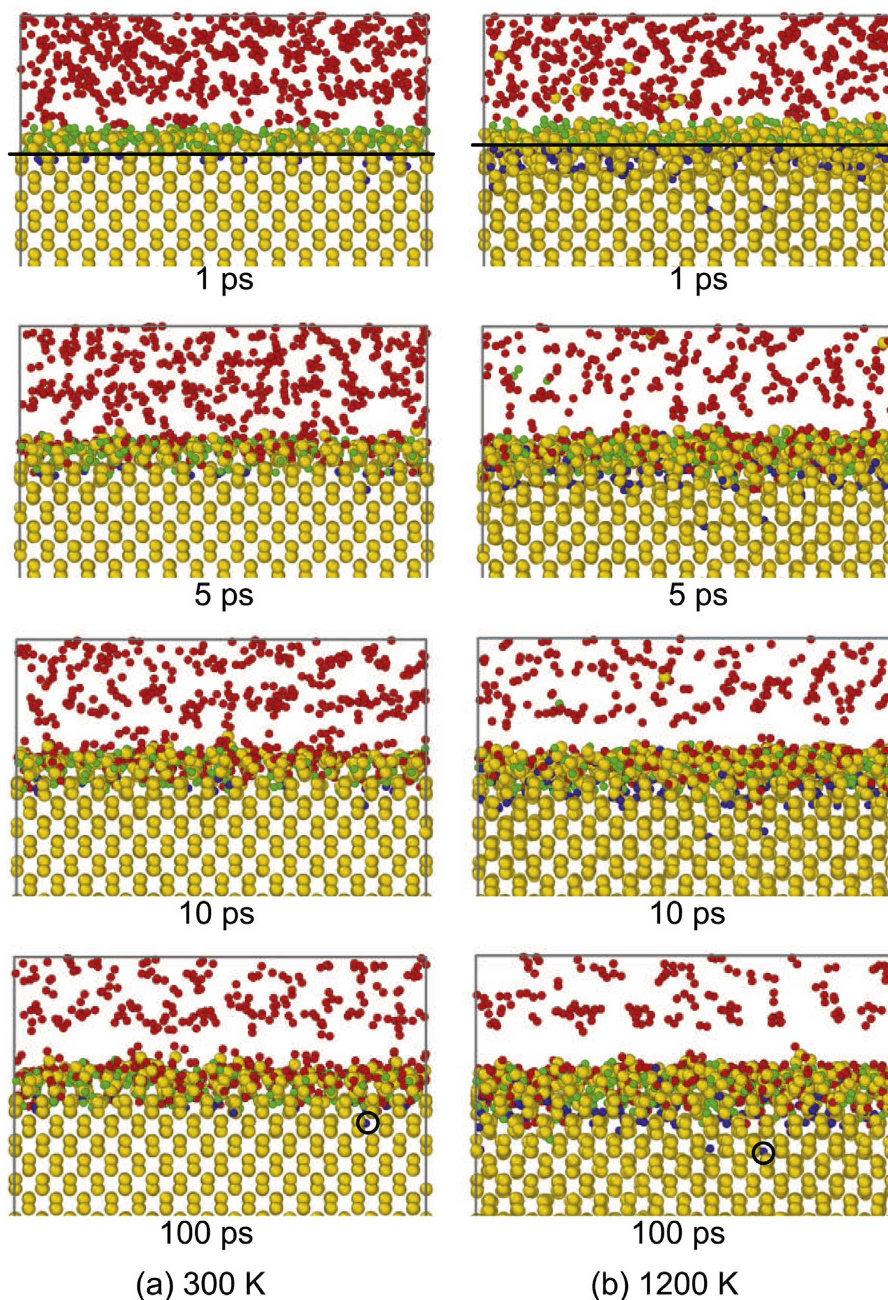

Fig. 3. The evolution of atomistic structures during oxidation process under 300 K and 1200 K. A line marked on configuration at 1 ps divides the surface region and deeper layers. The O atoms in surface region are tracking by green whereas in deeper layers as blue. The O atoms transported into Si after 1 ps are represented as red. (For interpretation of the references to color in this figure legend, the reader is referred to the web version of this article.)

Firstly, the Si structure was relaxed to obtain the stable configuration of bulk Si with (100) free surface. Si bulk with (100) free surface was thermalized under 300 K for 60 ps in NVT (Canonical) ensemble, subsequently relaxed in NVE (micro-canonical) ensemble for 20 ps, with time step as 0.5 fs [31]. After relaxation, the surface dimers were observed in (100) surface along ⟨110⟩ directions. The side view and top view of the relaxed configuration with surface dimers are shown in Fig. 1. Atoms with orange color represent the dimer structures. Then, to investigate the oxidation process, top and bottom space of the simulation box were randomly filled with O_2 molecules, as shown in Fig. 2(a). Initial oxygen gas pressure was approximately 298 atm, corresponding to numbers of O_2 molecules as 800. Such pressure value was set much higher than the value in experiments to accelerate the oxidation so that the early stage oxidation was completed in the ReaxFF MD simulation time scale, e.g. nanosecond [3]. Before oxidation, in order to well distribute O_2 molecules in the simulation box, the hybrid configuration was relaxed at 100 K for 1 ps, which is similar to the procedure in the previous literature [42]. Then, the temperature of the whole system was set as 300 K, 500 K, 700 K, 1000 K and 1200 K, controlled by NVT ensemble with a temperature damping constant of 10 fs. Time step for oxidation was 0.1 fs. The NVT ensemble was performed by Nose–Hoover heat bath.

Due to the free surface and interaction between Si and O, there was residual stress distributed in Si bulk. Here, the stress was calculated as the volume average of the per-atom virial stress in a slab perpendicular to z direction with a thickness of 1.296 Å (half of the oxide layer thickness) [27,31]. We calculated the residual stress dis-

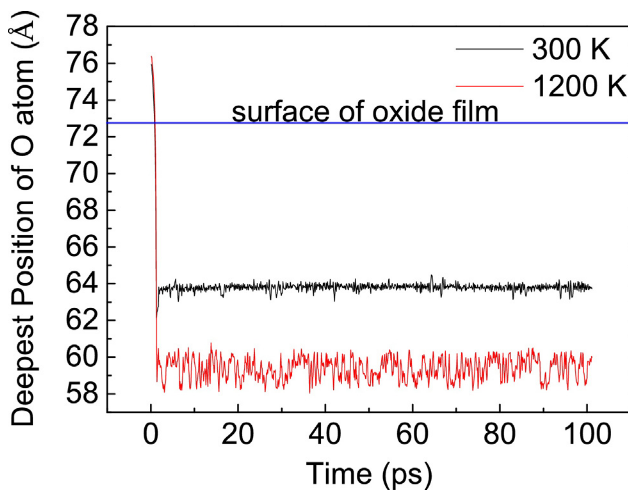

Fig. 4. Tracking of O atom with the deepest position (marked by a circle in Fig. 3) during oxidation process under 300 K and 1200 K.

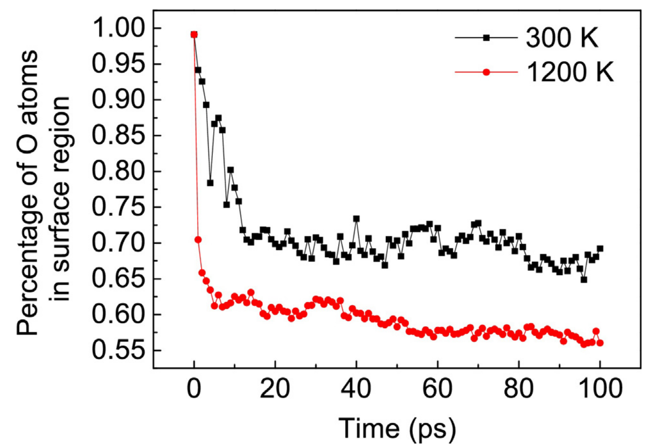

Fig. 5. The percentage of O atoms in surface region with respect to the total O atoms in the oxide film during oxidation process under 300 K and 1200 K.

tribution along *z* direction away from (100) free surface. The related distribution of *x* and *y* component normal stress $\sigma^{initial}$ is shown in Fig. 2(b). The *x* component $\sigma^{initial}$ was tensile one at the top five surface layers whereas it turned to compression from the sixth layer to the deeper layers. In contrast, *y* component one displayed slight compression in top five layers and approximately became zero at deeper region. Such anisotropic behavior may result from the surface dimer structures which were only binding along *x* direction, as shown in Fig. 1. To clarify the anisotropic effect, the distributions of both *x* and *y* component stress for the oxidized configurations were calculated by the same method in Section 3.

3. Results and discussion

3.1. Oxidation process

The evolution of atomistic structures during oxidation process under 300 K and 1200 K are shown in Fig. 3. Most of the O_2 molecules spontaneously dissociated into atoms when they were absorbed on Si(100) surface under both room temperature and 1200 K because the energy barrier of O_2 dissociation is extremely low which can be easily overcome by the energy gain from oxygen chemisorption on Si(100) surface [5,43–47]. At the initial instant (1 ps), there was already a large amount of O atoms transporting into Si bulk. Here, we define the top three layers of oxide film as surface region (approximately 3.9 Å), and the O atoms in surface region at instant 1 ps are represented as green color whereas the O atoms in deeper layers are represented as blue color as separated by the a line in Fig. 3. The O atoms transported into Si after 1 ps are represented as red color, which mainly accumulated in the surface region. In the final configuration (100 ps), most of O atoms locating at the deeper region were still those transported at the starting moment. Such phenomenon was more obvious under 1200 K.

The O atom which is located in the deepest layer at 100 ps is tracked (marked by a circle in Fig. 3). The position of it during oxidation is shown in Fig. 4. It is obvious that O atom ballistically went to the deepest position at initial instant (approximately 9 Å respect to the film surface under 300 K and 14 Å under 1200 K). Afterwards, it remained at similar depth, while slightly fluctuated under 1200 K due to thermal effect.

The percentage of O atoms in surface region with respect to the total O atoms in the oxide film during the oxidation process has been shown in Fig. 5. Diffusion of O atoms into deeper region mainly occurred before the first 10 ps for both of conditions under 300 K and 1200 K. After that, the percentage of O atoms within surface region stayed as nearly 70% of total oxide film under 300 K while 60% under 1200 K. Indeed, the early stage oxidation was almost completed in 10 ps. It was reported that the ballistic transport acted as one possible mechanism for ultrathin film rather than the conventional dissolution-diffusion, supporting by both experiment and simulations [5,34,35]. Our results found that the accumulation of O atoms at surface region may generate compressive stress at the surface region and further block O atom diffusion into deeper layers, accordingly the ballistic transport of O atoms at very early moment played dominant role during oxidation of Si.

3.2. Competition between thermal actuation and compressive stress blocking

The diffusion of O atom can be facilitated by thermal effect, whereas hindered due to the blocking of compression at surface region. To unravel the O atom transport mechanism during early stage of oxidation, the distributions of O atoms and σ along *z* direction at 100 ps for different temperatures ranging from 300 K to 1200 K were calculated, as shown in Fig. 6. Since the normal stress in *x* and *y* directions was anisotropic at initial state as Fig. 2(b), both of the *x* and *y* component normal stresses at 100 ps are shown in Fig. 6. In order to eliminate the influence of thermal fluctuation to the distributions of O atoms and σ, every data point in Fig. 6 was averaged during last 5 ps. For all the temperature values, O concentration reached maximum at second or third layer from surface then reduced at deeper layers. Besides, the stress distributions presented similar tendency, all of which displayed compressive stress in the surface region. The maximum compression stress located at the region with the maximum O concentration. Due to the injection of O atoms, the oxide film turned to expand in *x* and *y* directions. But, as the lateral expansion was constrained by the Si substrate, compression stress was generated in the oxide film. Moreover, the compression stress of *x* component under all temperatures was slightly lower than that of the *y* component one at top five layers. This may be attributed to the superposition of the compressive stress generated by the O atoms injection during oxidation and the *x* component residual tension leading by the initial free surface of Si (shown in Fig. 2). After the maximum compression stress position, the stress gradually increased to become a tensile stress at the interface of Si and SiO_x. Since both *x* and *y* component stress were tension stresses with quite similar values at the interface between Si and SiO_x, we ascribed that the tensile stress was generated by the mismatch between the growth strain in Si and SiO_x. Below the interface region, *y* component stress turned

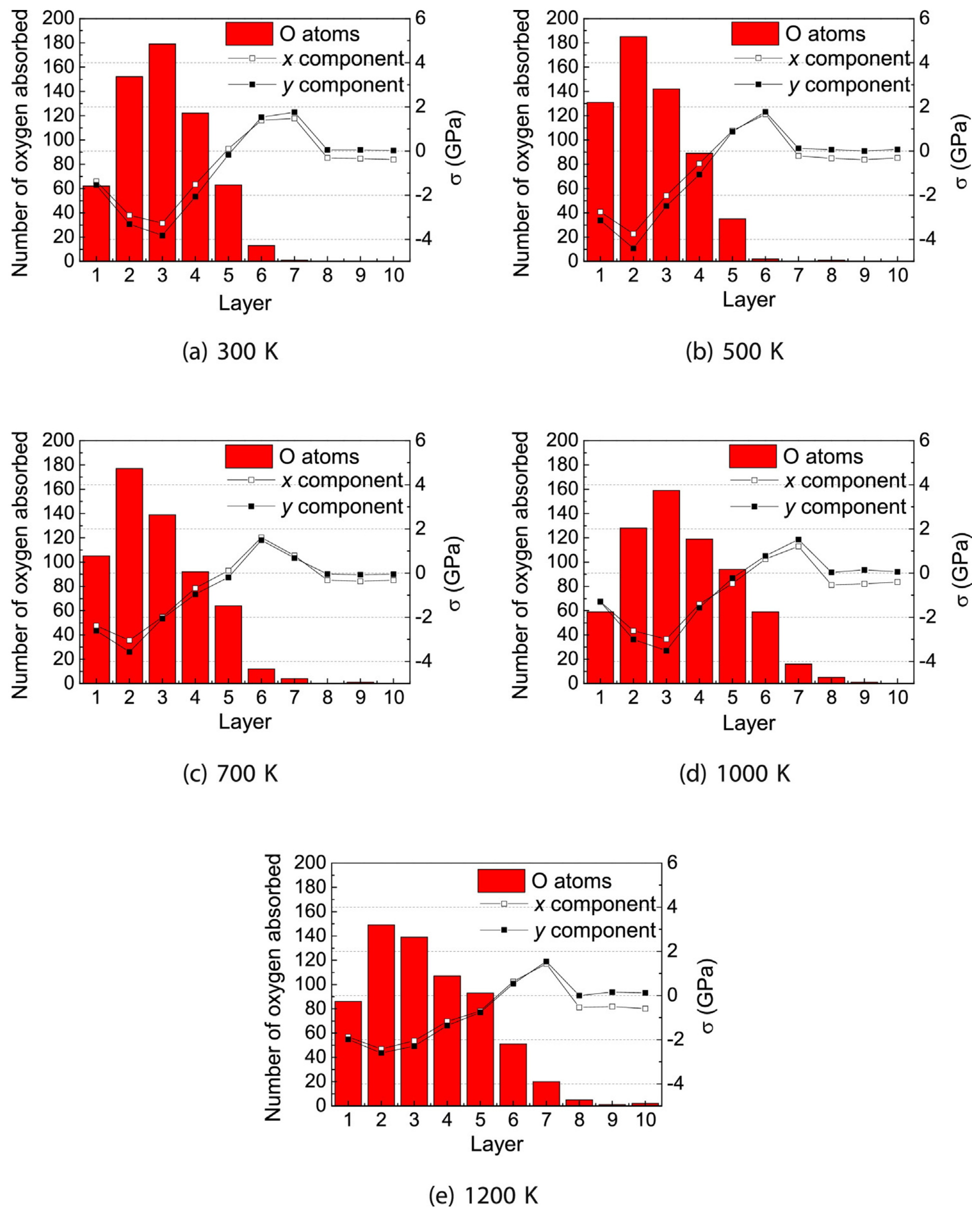

Fig. 6. Oxygen distribution in oxide film (column graph) and the corresponding *x* and *y* component stress distribution (line and symbol graph) after oxidation for 100 ps under different temperatures.

to be zero while *x* component one appeared as a small compressive value, owning to the initial compression of *x* component in these layers as well. Therefore, both of the initial residual stress and the growth stress played roles on the stress distribution of the oxidized structures. From Fig. 6, it is shown that under low temperature the maximum O concentration and compression stress were higher at surface region, while the O concentration at deeper layer was lower. Thus, the micromechanism of Si(100) oxidation can be described as the ballistically transport of O atoms into the surface region at the very beginning of oxidation (~1 ps) generating high O concentration and compression stress at the surface layer which blocked subsequent O transport. But, under high temperature, thermal actuation promoted the O transport into deeper layer, so that higher O concentration at deeper layer was observed. Hence, we concluded that the O transport was primarily controlled by the competition between thermal actuation and compression stress blocking.

Furthermore, the time evolution of average stress at surface region was calculated by taking *x* component as an example for different temperatures, as shown in Fig. 7. At the beginning of oxidation, there was slight tensile stress due to the initial residual tension of *x* component, approximately 0.89 GPa. With oxidation proceeding, it turned to be compression of which the value increased greatly, then after 40 ps the compression remained and finally reached to the range of 2.0–3.0 GPa at 100 ps. The compressive stress was larger under low temperature comparing with that under high temperature. Since O atoms could transport into deeper layers by thermal actuation, the compression blocking was weakened under higher temperature. Recent research on self-limiting oxidation mechanism of small-diameter Si nanowires demonstrated that the interfacial compressive stress was relatively high under low temperature and therefore responsible for self-limited oxidation [4,48]. These previous results could be explained by the

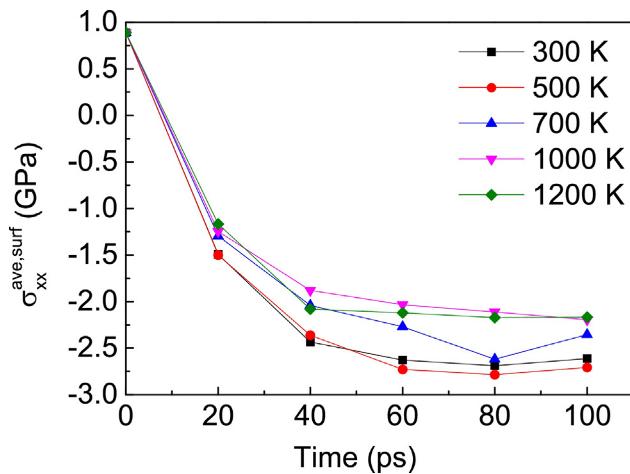

Fig. 7. Time evolution of average stress in the surface region during oxidation process under different temperatures.

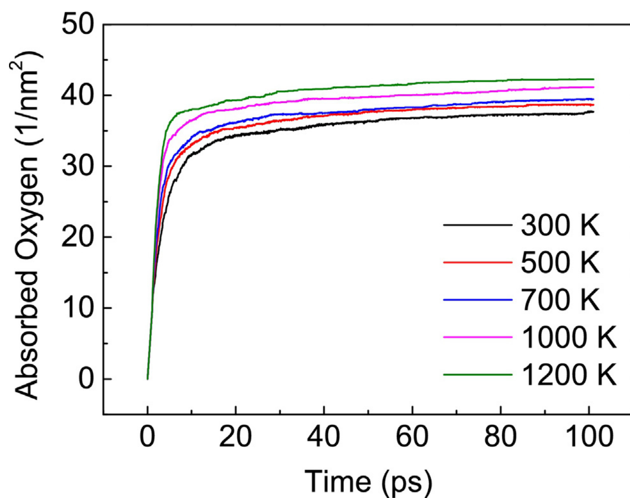

Fig. 8. Numbers of absorbed O atoms into oxide film during oxidation process under different temperatures.

competition mechanism between thermal actuation and compressive stress blocking proposed by the present work.

Fig. 8 shows the numbers of O atoms absorbed into per unit area of Si bulk during oxidation for different temperatures. The curves have similar shape, all of which indicate that the oxygen consumption was steeply increasing from 0 ps to 10 ps and slowed up until about 30 ps then nearly kept unchanged afterwards. The slopes reflected the reaction rate, which present that oxidation rate was extremely high in the first 10 ps. After the first 10 ps, oxidation was decelerating attributed to the blocking of compression at surface region. Comparison with different temperatures shows that both of the oxygen consumption and oxidation rate were increased by temperature rise owning to thermal actuation effect.

3.3. Quality of oxide film

Silicon-based devices such as metal-oxide-semiconductor transistors require a Si/SiO_x interface with flat morphology and low defect density [49]. The chemical state of the suboxide layers including Si^+, Si^{2+} and Si^{3+} also affects the performance of these devices, especially when the scale reduces to nanometers [50]. To analysis the film quality, the morphology of interface was characterized by means of root-mean-square (RMS) roughness, which was calculated as

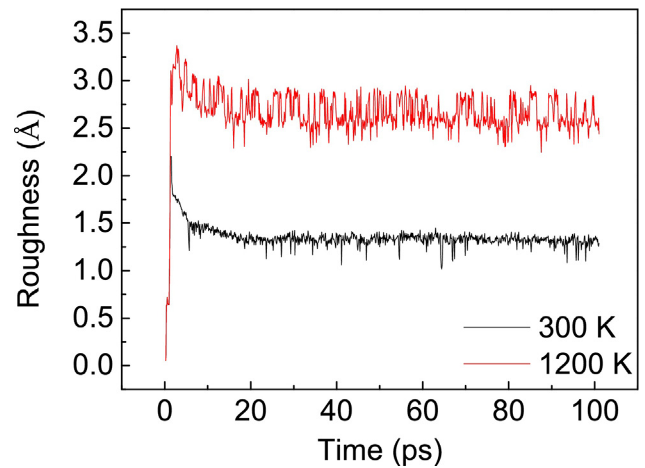

Fig. 9. Si/SiO_x interface roughness during oxidation process under 300 K and 1200 K.

$$\delta = \sqrt{\langle (h - \bar{h})^2 \rangle} \quad (1)$$

where h is the z-coordinate of each Si atom nearest to the interface without O neighbors, and $\bar{h}$ is the average over all h values [31]. Fig. 9 shows that the roughness rapidly increased at the very beginning of oxidation then slightly reduced until 10 ps, after that remained at nearly 1.5 Å under 300 K while 2.7 Å with more notable fluctuation under 1200 K. The interface morphology was smoother under 300 K thanks to the effect of compression blocking at surface region which restricted O transport. Under 1200 K, the interface turned to rougher because of the thermal actuation. The difference has been reflected by the atomistic configurations in Fig. 3 as well. Other experiment and first-principles studies also indicated that thermal oxidation under lower temperature could lead to the formation of a well-controlled uniform oxide layer [51,21], in accordance with our results.

The stoichiometry profiles of final configurations under 300 K and 1200 K are shown in Fig. 10. Different colors denote Si^{4+}, Si^{3+}, Si^{2+}, Si^+, and Si crystal which were calculated by the number of nearest oxygen neighbors. From Fig. 10(a) and (b), it shows that there were more Si^{4+} and Si^{3+} at surface layers under 300 K comparing with 1200 K, which means that more O atoms accumulated near surface region and formed a more complete oxidized structure. The total numbers of Si^{2+}, Si^{3+} and Si^{4+} were also larger under 300 K than that under 1200 K, whereas Si^+ was in contrast, as shown in Fig. 10(c). Mauludi et al. found that number of Si^+ decreased while numbers of Si^{2+}, Si^{3+} and Si^{4+} increased with oxidation proceeding under 300 K leading to a better quality film, in agreement with the present work [5].

In this simulation, the kinetic energy was suddenly given to the atoms for each temperature. Besides, extremely high pressure was applied to speed up the reaction rate, and the pressure was decreasing rapidly with consumption of oxygen gas. To validate the effect of initial kinetic energy and oxygen pressure, we have also simulated the oxidation by linearly increasing the temperature with same heating rate to 300 K and 1200 K then holding on until 100 ps. Under linear heat treatment, kinetic energy of O atoms was gradually increased and the pressure of oxygen gas was decreased with a lower rate as well. The corresponding evolution of atomistic structures during oxidation proceeding appeared similarly as that by suddenly setting to the target temperature, indicating that the ballistic transport of O atoms at initial instant was not influenced by the heat treatment and the gas pressure. The quantitative analy-

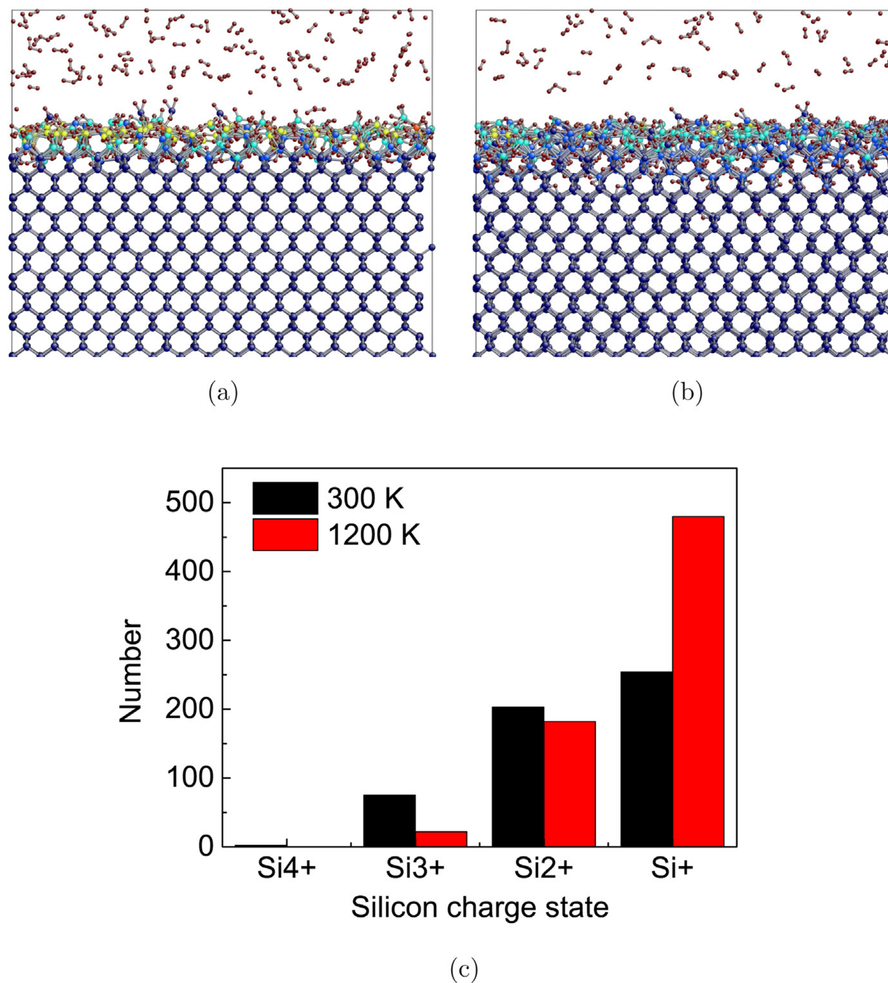

Fig. 10. Si charge state in oxide film after oxidation for 100 ps under (a) 300 K and (b) 1200 K. Red, orange, yellow, light blue, blue and dark blue atoms denote oxygen, Si^{4+}, Si^{3+}, Si^{2+}, Si^{+}, and Si crystal, respectively. (c) Numbers of Si^{4+}, Si^{3+}, Si^{2+} and Si^{+} corresponding to (a) and (b). (For interpretation of the references to color in this figure legend, the reader is referred to the web version of this article.)

sis on the effect of oxygen pressure will be presented in our future works.

4. Conclusions

By a ReaxFF MD simulation study, the transport of O atoms was found to control the initial oxidation stage of Si. High O concentration was induced by the transport of O atoms into surface region at the very beginning of oxidation (~1 ps), leading to compression stress of the surface layer which blocked the subsequent transport of O. Nevertheless, the transport of O could be promoted by thermal actuation under high temperature. Therefore, the oxidation rate and absorbed O atoms were enhanced with temperature increase. O atoms had greater possibility to go deeper inward, generating a higher O concentration in deep layers and releasing the surface compression. Consequently, a rough interface with less stoichiometric oxide structure was formed under 1200 K while the quality of the oxide film was much better at room temperature. We believe that the mechanism discovered in this work suggests a general way to explain other self-limiting oxidation behaviors, and is meaningful for both material science and applications in electronics.

Acknowledgements

This work was supported by National Natural Science Foundation of China (grant numbers 11402206, 51421004 and 51505364) and Scientific Research Program of Shaanxi Province (grant number 2015JM1021).

References

[1] A. Yoshigoe, K. Moritani, Y. Teraoka, Real time observation of initial thermal oxidation using O_2 gas on Si(001) surface by means of synchrotron radiation Si-2p photoemission spectroscopy, Appl. Surf. Sci. 216 (1–4) (2003) 388–394.
[2] A. Yoshigoe, Y. Teraoka, Time resolved photoemission spectroscopy on Si(001)-2 × 1 surface during oxidation controlled by translational kinetic energy of O_2 at room temperature, Surf. Sci. 532 (3) (2003) 690–697.
[3] B.H. Kim, M.A. Pamungkas, M. Park, G. Kim, K.R. Lee, Y.C. Chung, Stress evolution during the oxidation of silicon nanowires in the sub-10 nm diameter regime, Appl. Phys. Lett. 99 (14) (2011) 143115.
[4] U. Khalilov, G. Pourtois, A.C.T.V. Duin, E.C. Neyts, Self-limiting oxidation in small-diameter Si nanowires, Chem. Mater. 24 (11) (2012) 2141–2147.
[5] M.A. Pamungkas, M. Joe, B.H. Kim, K.R. Lee, Reactive molecular dynamics simulation of early stage of dry oxidation of Si(100) surface, J. Appl. Phys. 110 (5) (2011) 053513.
[6] M.A. Pamungkas, B.H. Kim, K.R. Lee, Reactive molecular dynamic simulations of early stage of wet oxidation of Si(001) surface, J. Appl. Phys. 114 (7) (2013) 073506.
[7] T. Engel, The interaction of molecular and atomic oxygen with Si(100) and Si(111), Surf. Sci. Rep. 18 (4) (1993) 93–144.
[8] H. Cui, C.X. Wang, G.W. Yang, D. Jiang, Origin of unusual rapid oxidation process for ultrathin oxidation (<2 nm) of silicon, Appl. Phys. Lett. 93 (20) (2008) 203113.
[9] Y. Takakuwa, F. Ishida, T. Kawawa, Phase transition from Langmuir-type adsorption to two-dimensional oxide island growth during oxidation on Si(001) surface, Appl. Surf. Sci. 216 (1) (2003) 133–140.

[10] K. Nakajima, Y. Okazaki, K. Kimura, Initial oxidation process on Si(001) studied by high-resolution Rutherford backscattering spectroscopy, Phys. Rev. B 63 (11) (2001) 263–271.
[11] A. Bongiorno, A. Pasquarello, Atomistic model structure of the Si(100)-SiO_2 interface from a synthesis of experimental data, Appl. Surf. Sci. 234 (1) (2004) 190–196.
[12] H. Noma, H. Takahashi, H. Fujioka, M. Oshima, Y. Baba, K. Hirose, M. Niwa, K. Usuda, N. Hirashita, Uniaxial and biaxial strain field dependence of the thermal oxidation rate of silicon, J. Appl. Phys. 90 (10) (2001) 5434–5437.
[13] J.Y. Yen, C.H. Huang, J.G. Hwu, Effect of mechanical stress on characteristics of silicon thermal oxides, Jap. J. Appl. Phys. 41 (1) (2002) 81–82.
[14] A. Mihalyi, R.J. Jaccodine, T.J. Delph, Stress effects in the oxidation of planar silicon substrates, Appl. Phys. Lett. 74 (14) (1999) 1981–1983.
[15] M. Lin, R.J. Jaccodine, T.J. Delph, Planar oxidation of strained silicon substrates, J. Mater. Res. 16 (3) (2001) 728–733.
[16] J.Y. Yen, J.G. Hwu, Stress effect on the kinetics of silicon thermal oxidation, J. Appl. Phys. 89 (5) (2001) 3027–3032.
[17] J.Y. Yen, J.G. Hwu, Enhancement of silicon oxidation rate due to tensile mechanical stress, Appl. Phys. Lett. 76 (14) (2000) 1834–1835.
[18] M. Yata, Y. Uesugisaitow, M. Kitajima, A. Kubo, V.E. Korsukov, Effects of strain on the dissociation dynamics of O_2 on Si(001), Phys. Rev. Lett. 91 (20) (2003) 1160–1166.
[19] M. Yata, External stress-induced chemical reactivity of O_2 on Si(001), Phys. Rev. B 81 (20) (2010) 205402.
[20] M. Yata, Effects of external strain on the order–disorder phase transition and the hierarchical structure on the Si(001) surface, Phys. Rev. B 74 (16) (2006) 165407.
[21] H. Kageshima, K. Shiraishi, First-principles study of oxide growth on Si(100) surfaces and at SiO_2/Si(100) interfaces, Phys. Rev. Lett. 81 (26) (1998) 5936–5939.
[22] A. Pasquarello, M.S. Hybertsen, R. Car, Interface structure between silicon and its oxide by first-principles molecular dynamics, Nature 396 (5) (1998) 58–60.
[23] T. Yamasaki, C. Kaneta, T. Uchiyama, T. Uda, K. Terakura, Geometric and electronic structures of SiO_2/Si(001) interfaces, Phys. Rev. B 63 (11) (2001) 115314.
[24] T. Yamasaki, K. Kato, T. Uda, Oxidation of the Si(001) surface: lateral growth and formation of P(b0) centers, Phys. Rev. Lett. 91 (14) (2003) 146102.
[25] N. Takahashi, T. Yamasaki, C. Kaneta, Molecular dynamics study of Si(100)-oxidation: SiO and Si emissions from Si/SiO_2 interfaces and their incorporation into SiO_2, J. Appl. Phys. 115 (22) (2014) 224303.
[26] S. Takamoto, T. Kumagai, T. Yamasaki, T. Ohno, C. Kaneta, A. Hatano, S. Izumi, Charge-transfer interatomic potential for investigation of the thermal-oxidation growth process of silicon, J. Appl. Phys. 120 (16) (2016) 165109.
[27] U. Khalilov, E.C. Neyts, G. Pourtois, A.C.T.V. Duin, Can we control the thickness of ultrathin silica layers by hyperthermal silicon oxidation at room temperature? J. Phys. Chem. C 115 (50) (2011) 24839–24848.
[28] E.C. Neyts, U. Khalilov, G. Pourtois, A.C.T.V. Duin, Hyperthermal oxygen interacting with silicon surfaces: adsorption, implantation, and damage creation, J. Phys. Chem. C 115 (11) (2011) 4818–4823.
[29] H. Cao, M.A. Pamungkas, B.H. Kim, K.R. Lee, A molecular dynamics simulation study on the initial stage of Si(001) oxidation under biaxial strain, J. Nanosci. Nanotechnol. 13 (2) (2013) 1074–1077.
[30] U. Khalilov, G. Pourtois, A.C.T.V. Duin, E.C. Neyts, Hyperthermal oxidation of Si(100)2 $\times$ 1 surfaces: effect of growth temperature, J. Phys. Chem. C 116 (15) (2012) 8649–8656.
[31] A. Armigliato, R. Balboni, S. Frabboni, On the c-Si|α-SiO_2 interface in hyperthermal Si oxidation at room temperature, J. Phys. Chem. C 116 (41) (2012) 21856–21863.
[32] U. Khalilov, G. Pourtois, S. Huygh, A.C.T.V. Duin, E.C. Neyts, A. Bogaerts, New mechanism for oxidation of native silicon oxide, J. Phys. Chem. C 117 (19) (2013) 9819–9825.
[33] J. Wen, T. Ma, W. Zhang, G. Psofogiannakis, A.C.T.V. Duin, L. Chen, L. Qian, Y. Hu, X. Lu, Atomic insight into tribochemical wear mechanism of silicon at the Si/SiO_2 interface in aqueous environment: molecular dynamics simulations using ReaxFF reactive force field, Appl. Surf. Sci. 390 (2016) 216–223.
[34] T. Yasuda, N. Kumagai, M. Nishizawa, S. Yamasaki, H. Oheda, K. Yamabe, Layer-resolved kinetics of Si oxidation investigated using the reflectance difference oscillation method, Phys. Rev. B 67 (19) (2003) 195338.
[35] A.A. Demkov, O.F. Sankey, Growth study and theoretical investigation of the ultrathin oxide SiO_2-Si heterojunction, Phys. Rev. Lett. 83 (10) (1999) 2038–2041.
[36] R.K. Agrawal, M. Yunis, Theory of static structural properties, crystal stability, and phase transformations: application to Si and Ge, Phys. Rev. B 26 (10) (1982) 5668–5687.
[37] M.A. Hopcroft, W.D. Nix, T.W. Kenny, What is the Young's modulus of silicon? J. Microelectromech. Syst. 19 (2) (2010) 229–238.
[38] S.A.P.A.Y.G.H.M. Aktulga, J.C. Fogarty, Parallel reactive molecular dynamics: numerical methods and algorithmic techniques, Parallel Comput. 38 (2012) 245–259.
[39] S. Plimpton, Fast parallel algorithms for short-range molecular dynamics, J. Comput. Phys. 117 (1) (1995) 1–19.
[40] M.J. Buehler, A.C.T.V. Duin, G.W. Rd, Multiparadigm modeling of dynamical crack propagation in silicon using a reactive force field, Phys. Rev. Lett. 96 (9) (2006) 095505.
[41] S. Dumpala, S.R. Broderick, U. Khalilov, E.C. Neyts, A.C.T.V. Duin, J. Provine, R.T. Howe, K. Rajan, Integrated atomistic chemical imaging and reactive force field molecular dynamic simulations on silicon oxidation, Appl. Phys. Lett. 106 (1) (2015) 011602.
[42] D.A. Newsome, D. Sengupta, H. Foroutan, M.F. Russo, A.C.T.V. Duin, Oxidation of silicon carbide by O_2 and H_2O: a ReaxFF reactive molecular dynamics study – Part I, J. Phys. Chem. C 116 (2012) 16111–16121.
[43] Y. Miyamoto, A. Oshiyama, Atomic and electronic structures of oxygen on Si(100) surfaces: metastable adsorption sites, Phys. Rev. B 41 (18) (1990) 12680–12686.
[44] K. Kato, T. Uda, Chemisorption of a single oxygen molecule on the Si(100) surface: initial oxidation mechanisms, Phys. Rev. B 62 (23) (2000) 15978–15988.
[45] A. Bongiorno, A. Pasquarello, Reaction of the oxygen molecule at the Si(100)-SiO_2 interface during silicon oxidation, Phys. Rev. Lett. 93 (8) (2004) 086102.
[46] L.C. Ciacchi, M.C. Payne, First-principles molecular-dynamics study of native oxide growth on Si(001), Phys. Rev. Lett. 95 (19) (2005) 196101.
[47] N. Richard, A. Estve, M. Djafari-Rouhani, Density functional theory investigation of molecular oxygen interacting with Si(100)-(2 $\times$ 1), Comput. Mater. Sci. 33 (2005) 26–30.
[48] U. Khalilov, G. Pourtois, A. Bogaerts, A.C.T.V. Duin, E.C. Neyts, Reactive molecular dynamics simulations on SiO_2-coated ultra-small Si-nanowires, Nanoscale 5 (2) (2013) 719–725.
[49] T. Uchiyama, M. Tsukada, Atomic and electronic structures of oxygen-adsorbed Si(001) surfaces, Phys. Rev. B 53 (12) (1996) 7917–7922.
[50] J.H. Oh, H.W. Yeom, Y. Hagimoto, K. Ono, M. Oshima, N. Hirashita, M. Nywa, A. Toriumi, A. Kakizaki, Chemical structure of the ultrathin SiO_2/Si(100) interface: an angle-resolved Si 2*p* photoemission study, Phys. Rev. B 63 (63) (2001) 797–801.
[51] H. Watanabe, K. Kato, T. Uda, K. Fujita, M. Ichikawa, T. Kawamura, K. Terakura, Kinetics of initial layer-by-layer oxidation of Si(001) surfaces, Phys. Rev. Lett. 80 (80) (1998) 345–348.